Nano Self-Assembly of Recombinant Human Gelatin Conjugated with α-Tocopheryl Succinate for Hsp90 Inhibitor, 17-AAG, Delivery

Young-Wook Won,[†] Sun-Mi Yoon,[†] Chung Hee Sonn,[‡] Kyung-Mi Lee,[‡,*] and Yong-Hee Kim[†,*]

[†]Department of Bioengineering, Institute for Bioengineering and Biopharmaceutical Research, Hanyang University, 17, Haengdang-dong, Seongdong-gu, Seoul, 133-791, Republic of Korea, and [‡]Department of Biochemistry and Division of Brain Korea 21 Program for Biomedical Science, Korea University College of Medicine, Seoul, Republic of Korea

ABSTRACT A wide variety of drug delivery systems have been developed for the delivery of anticancer agents. One of the most frequently used natural biomaterials in drug delivery systems is polysaccharides; however, they are difficult to digest and to eliminate from the body after systemic administration due to their high molecular weight natures and the absence of degrading enzymes. Therefore, the development of degradable and eliminable natural biomaterials is critical for successful *in vivo* applications. In the present study, we report the development of self-assembled biodegradable nanoparticles based on recombinant human gelatin (rHG) modified with alpha-tocopheryl succinate (TOS). The rHG-TOS nanoparticles efficiently encapsulated 17-AAG (17-allylamino-17-demethoxygeldanamycin), a small molecular anticancer drug targeting heat shock protein 90. The formation of 17-AAG-loaded nanoparticles was confirmed using TEM and dynamic light scattering analysis and found to be within the size of 90—220 nm. The loading efficiency, sustained release pattern, and stability of 17-AAG from the rHG-TOS nanoparticles were determined using HPLC. Furthermore, the passive targeting of rHG-TOS nanoparticles to the tumor area *via* enhanced permeability and retention effect was examined by noninvasive live animal imaging in a tumor mouse model. Finally, the 17-AAG-loaded nanoparticles were nonimmunogenic and more efficient than free 17-AAG in manifesting an anticancer effect in the tumor model. Overall, our data demonstrate rHG-TOS as a promising tool for the delivery of 17-AAG featuring therapeutic efficacy and biocompatibility.

KEYWORDS: anticancer drug delivery · nanoparticles · recombinant human gelatin · 17-AAG · self-assembly · alpha-tocopheryl succinate

In recent decades, there has been increased interest in the development of drug delivery systems including nanoparticles, polymeric micelles, liposomes, and injectable gels. In particular, self-assembled nanoparticles are attractive tools since they possess a characteristic of encapsulating lipophilic anticancer agents during the spontaneous formation of nanoassembly in an aqueous solution.[1] In addition, nanoparticles have the advantages of achieving passive targeting of the tumor *via* enhanced permeability and retention (EPR) effects and avoiding reticuloendothelial system (RES) uptake due to the hydrophilic surface.[2] Various hydrophilic natural polymers including polysaccharides and proteins were modified into amphiphilic polymers through the conjugation of hydrophobic molecules.[3] Among them, considerable attention has been focused on gelatin because it has been widely used in pharmaceutical industries due to its nontoxicity, biodegradability, and biocompatibility. Recently, recombinant human gelatin (rHG) manufactured by splicing recombinant human collagen, one of the most abundant proteins in the body, was used to prepare nanoparticles for protein delivery.[4] Since rHG is nontoxic and useful for developing nanostructures due to its nonimmunogenicity and the homogeneity in molecular weight, we assumed that it was a good biomaterial to use as a hydrophilic backbone for the manufacture of self-assembled nanoparticles.

Hydrophobic molecules are key components in the fabrication of amphiphilic polymers; therefore, they should be nontoxic, biocompatible, and nonimmunogenic in *in vivo* applications. In addition, their degradability and stability in the body need to be considered since hydrophobic molecules play crucial roles in the size and stability of nanoparticles, encapsulation of drugs, and rigidity in nanostructures. Alpha-tocopheryl succinate (α-TOS), one of the vitamin analogues, is a well-known hydrophobic molecule composed of three domains: the functional domain, the signaling domain, and the hydrophobic domain.[5,6] The succinyl group in position C6 of the chromanol ring is cleaved through esterase-dependent hydrolysis, during which

* Address correspondence to yongheekim@hanyang.ac.kr, kyunglee@korea.ac.kr.

Received for review January 17, 2011 and accepted April 25, 2011.

Published online April 25, 2011
10.1021/nn200173u

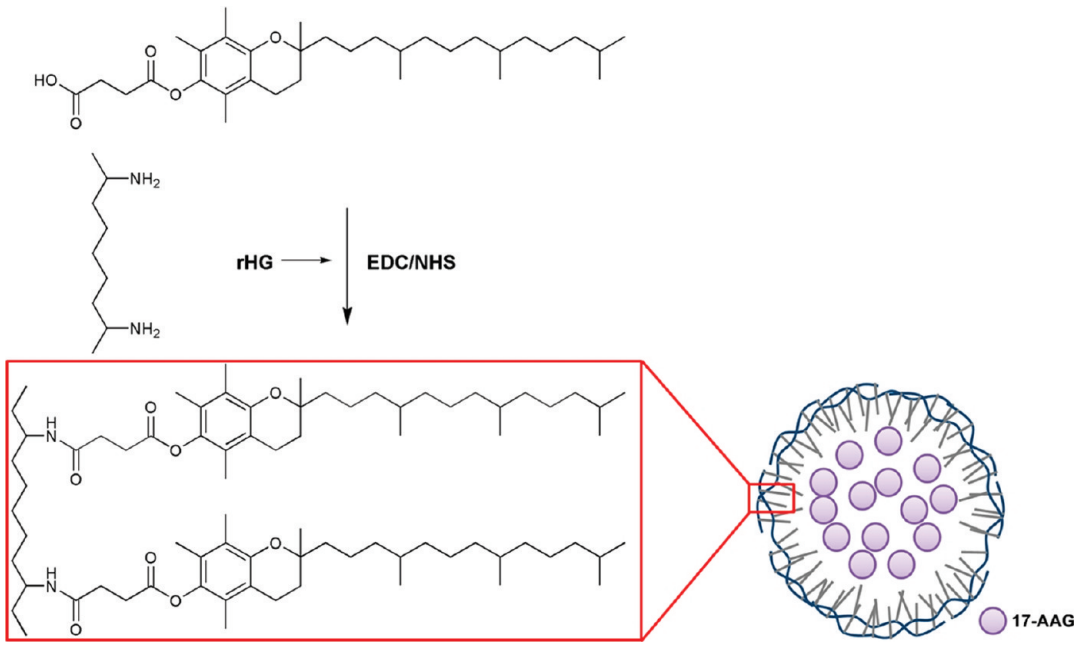

Figure 1. Schematic representation of the conjugation and a diagram of drug-loaded rHG-TOS nanoparticles.

α-TOS is completely converted into α-TOH.[6,7] When rHG is conjugated with α-TOS through an amide bond, the hydrophobic domain is exposed to the opposite side of the hydrophilic backbone; therefore, the conjugate easily forms nanoparticles in aqueous environments. During the process, lipophilic anticancer agents can be encapsulated into the hydrophobic core of the nanoparticles. The hydrolysis may trigger the nanoparticle's disassembly and facilitates drug release.

Chemotherapy is a standardized regimen for the treatment of cancer patients after and/or before surgery. Fluorouracil, cyclophosphamide, doxorubicin, and docetaxel are well-known cytotoxic drugs developed to inhibit DNA replication or arrest cell cycles. Recent studies regarding cancer biology have demonstrated that heat shock protein 90 (Hsp90) can be a target for cancer therapy because (i) Hsp90 plays a crucial role in the maturation and stabilization of a wide range of oncogenic client proteins;[8−10] (ii) Hsp90 stabilizes its client proteins under the environmental conditions found in tumors such as hypoxia, low pH, and poor nutritional status;[11] (iii) Hsp90 comprises as much as 4−6% of total protein in tumor cells, in contrast to the 1−2% in normal cells;[12] (iv) Hsp90 isolated from tumor cells has an approximately 100-fold greater binding affinity to Hsp90 inhibitors than does Hsp90 derived from normal cells;[12,13] and (v) a number of Hsp90 inhibitors can be selectively accumulated in tumor cells due to the intrinsic properties of Hsp90.[11,12] The promising anticancer effects of Hsp90 inhibitors have been shown in preclinical and clinical evaluations when it is administered as a single agent and/or in combination with chemotherapy.[14]

Geldanamycin (GA), the first class of natural Hsp90 inhibitors, has a high binding affinity to the ATP-binding pocket in Hsp90.[15] Hsp90 captures its client proteins inside the two N-termini of the Hsp90 dimer, and the chaperone functions of Hsp90 occur upon ATP binding to the binding pocket. On the other hand, Hsp90 is not able to drive the chaperone cycles in the presence of Hsp90 inhibitors due to the competitive inhibition of ATP binding to the binding pocket.[16] The substitution leads to ubiquitination and proteasomal degradation of the client proteins, resulting in cell death.[17] Despite the potent anticancer effects of GA in preclinical studies, the high hepatotoxicity observed in animal models remains an obstacle to clinical trials.[18] Efforts to minimize the toxicity have resulted in the development of a series of GA derivatives that maintain the activity with less toxicity. Among them, 17-AAG (17-allylamino-17-desmethoxygeldanamycin) is under clinical trials and shows promising anticancer activity with an acceptable toxicity level.[19,20] However, low solubility in water and instability in solution continue to be a challenge for future clinical applications.

One of the solutions to improve the bioavailability of 17-AAG is the use of self-assembled nanoparticles. In the present study, we developed a conjugate of rHG and α-TOS (rHG-TOS) for the delivery of 17-AAG. The nanostructures of rHG-TOS were characterized using dynamic light scattering (DLS) for size measurement and TEM for the analysis of morphological properties. The encapsulation ability of 17-AAG, the release pattern of the drug, its cellular uptake, and its anticancer effects in cancer cells were confirmed. In addition, *in vivo* distribution of the rHG-TOS nanoparticles was visualized using noninvasive live animal imaging

techniques. Finally, anticancer effects and immunogenicities of the 17-AAG-loaded nanoparticles were investigated in an animal tumor model. We conclude that rHG-TOS can be a promising delivery vehicle for 17-AAG and/or other hydrophobic agents.

RESULTS AND DISCUSSION

The most frequently used natural biomaterials in the drug delivery systems are polysaccharides; however, they have disadvantages of degradation and elimination in the body. Chitosan, for example, is difficult to digest from circulation because the chitinase and chitosanase required for decomposition exist in the intestine but not in the blood.[21] In addition, the elimination of polysaccharide *via* glomerular filtration is restricted due to its high molecular weight.[22,23] Therefore, polysaccharides are considered not to be appropriate materials for systemic drug formulation. On the other hand, rHG is easily degraded by serum proteins, and the degradation product may be eliminated from the body through the renal route.[24] Recently, a wide variety of biological anticancer drugs have been reported; however, no delivery vehicles have been developed for those agents. Therefore, we developed a biodegradable and bioeliminable nanoassembled carrier based on rHG for the delivery of the biologically active anticancer drug 17-AAG.

The highly water-soluble rHG was successfully modified into an amphiphilic polymer by conjugating α-TOS as shown in the scheme of synthesis (Figures 1 and S1). To characterize the conjugates of rHG-TOS, the remaining amine groups in rHG-TOS modified with various feeding amounts of α-TOS were quantitatively determined through a TNBS assay, and the mean diameters in each condition were determined. A negative correlation of the remaining amine groups with the feeding amount of α-TOS was observed, and the size results with low feeding amounts did not meet the quality criteria (Table S1). This result was likely due to the low rigidity of the rHG-TOS since only a small amount of α-TOS was attached to rHG. The conjugation conditions that showed more than 60% modification and good quality in size measurements were further tested with regard to the encapsulation of 17-AAG for the assessment of drug loading capacities. A positive correlation between the substitution degree and the loading efficiency (LE) was observed in the modification range from 60% to 70%, and LE reached a plateau at 70% modification. On the basis of these results, the conjugation conditions that produced 70% substitution were chosen as the optimal conditions for the preparation of rHG-TOS in terms of rigidity and loading capability. At the optimal conditions, LE and loading contents (LC) were 65 ± 5.5% and 8 ± 0.3%, respectively.

Critical aggregation concentration (CAC), indicating the nanoparticle formation ability, is considered one of

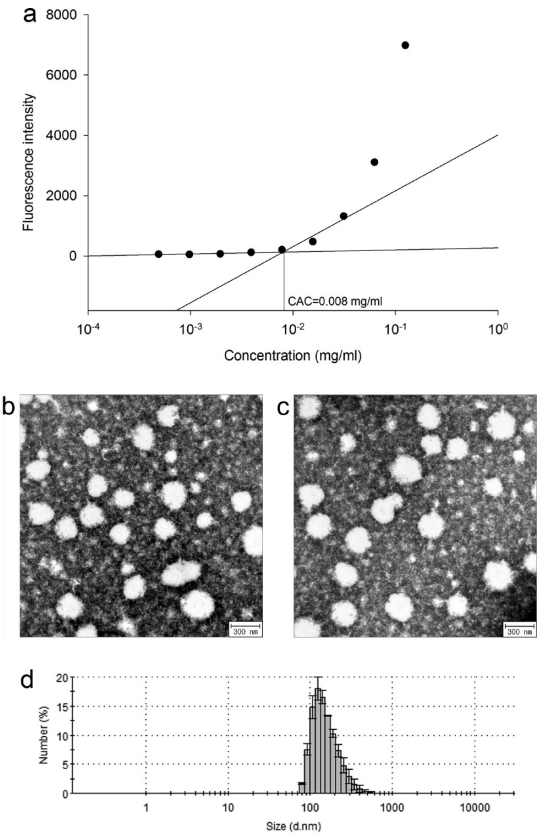

Figure 2. (a) Fluorometry probe-based CAC determination of rHG-TOS conjugates (CAC: ~0.008 mg/mL). TEM images of (b) unloaded rHG-TOS nanoparticles and (c) 17-AAG-loaded rHG-TOS nanoparticles. (d) Size distribution of 17-AAG-loaded rHG-TOS nanoparticles (data expressed as mean ± SD of three independent measurements).

the important factors required for amphiphilic materials to maintain nanostructures after systemic administration in the body due to the dilution in blood.[25,26] The amphiphilicity of rHG-TOS drives the spontaneous formation of nanoparticles composed of a hydrophilic outer shell and a hydrophobic inner core in aqueous environments. The CAC value of rHG-TOS was determined using DPH as a fluorometry probe. During the nanoparticle formation, intercalation of DPH into the hydrophobic core of rHG-TOS led to an increase in fluorescence intensity, as shown in Figure 2a. The fluorescence intensity of DPH increased dramatically near the rHG-TOS concentration of 0.008 mg/mL. The gradient of the plot increased sharply above that concentration, indicating nanoparticle formation. The formation of nanoparticles above the CAC value was confirmed before drug loading, and the effects of drug loading on nanoparticle formation were examined. The rHG-TOS nanoparticles were spherical in shape and well-dispersed without aggregation, demonstrating that rHG-TOS formed spherical nanoparticles in aqueous solution at a concentration higher than the CAC (Figure 2b). After 17-AAG loading, no changes were observed in the TEM micrograph (Figure 2c).

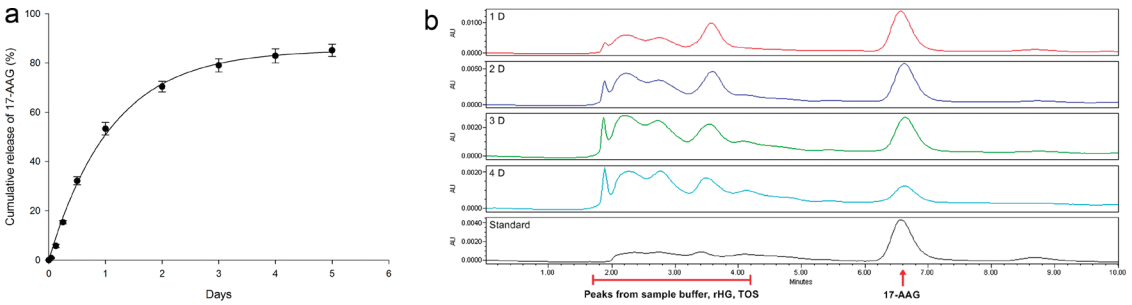

Figure 3. (a) *In vitro* release profile of 17-AAG from rHG-TOS nanoparticles at pH 7.4 and 37 °C under shaking at 100 rpm (data expressed as mean ± SD of three independent experiments with four replicates). (b) Stability of the released 17-AAG. HPLC was performed to quantify and evaluate the stability (red: 1 day, blue: 2 days, green: 3 days, sky blue: 4 days postrelease, black: 17-AAG standard). The retention time of 17-AAG is around 6.6 min under the test conditions.

In addition, a micrograph of the rHG-TOS nanoparticle with high magnification visualized using cryo-TEM confirms that rHG-TOS conjugates form a filled nanoparticle without bilayer (Figure S2). To further characterize the nanoparticles, the mean diameters of both nanoparticles were determined using DLS. The sizes of 17-AAG-unloaded and -loaded nanoparticles were measured to be 235 ± 41 and 239 ± 40 nm with polydispersity index (PDI) values of 0.266 ± 0.021 and 0.172 ± 0.019. The size distribution of 17-AAG-loaded nanoparticles analyzed from three independent TEM micrographs was measured to be 229 ± 42 nm (Figure 2c), and ~90% of nanoparticles were distributed in the size range from 90 to 220 nm, as shown in Figure 2d. TEM and DLS results demonstrated no influence of drug loading on nanoparticle formation.

The release profile of the encapsulated drug from the nanoparticle is crucial to the activity of the drug; moreover, the stability of the drug has to be maintained after the loading and release. Figure 3a shows the cumulative release profile of 17-AAG from the rHG-TOS nanoparticles at physiological pH and temperature under shaking. The *in vitro* release pattern of 17-AAG was biphasic and composed of an initial phase with rapid release and a second phase with slow, sustained release. Less than 1% of 17-AAG was released from the nanoparticles in the first 1 h, and the release reached ~5% for 3 h and ~30% for 12 h, suggesting no significant initial burst. After 24 h, ~50% of the 17-AAG was released from the nanoparticles, and up to ~70% was released within 48 h, when the second phase began. The rHG-TOS nanoparticles released 17-AAG for five days, achieving an ~80% total release. When the rigidity of rHG-TOS decreased, it was believed to facilitate the release of 17-AAG. The key molecule associated with rigidity is α-TOS, and the succinyl group in α-TOS is easily hydrolyzed under physiological environments.[27] Upon hydrolysis of α-TOS, the hydrophobic tail domain in α-TOS is detached from the rHG-TOS; hence the rHG-TOS losses its amphiphilicity. Consequently, the hydrolysis may lead to the disassembly of the nanoparticle structure, resulting in sustained release of drug. Regardless of the mechanism of drug release, the release kinetic is usually controlled by dissolution and/or diffusion.[28] Factors involved in the rate of drug release are diffusion coefficient of drug, effective surface area in the release media, drug solubility in the media, and the length of the diffusion path. A general equation based on the factors represents both the Noyes–Whitney law of dissolution and Fick's first law of diffusion. Consequently, dissolution and diffusion rate limited processes are considered to be a general release mechanism. The stability of released 17-AAG was confirmed using stability-indicating HPLC.[29,30] The retention time of 17-AAG remained constant at 6.6 min with the appearance of no other peaks representing degradation products of 17-AAG (Figure 3b). The rHG-TOS nanoparticles release 17-AAG long enough to circulate in the blood after systemic administration and maintain the stability of encapsulated 17-AAG during the release period.

Efficient cellular uptake in the disease area is a prerequisite for nanoparticles being used as a drug delivery system. In order to monitor the internalization of rHG-TOS, Cy5.5-labeled rHG-TOS was treated with squamous cell carcinoma (SCC) cells. Time-dependent trafficking of the nanoparticles was visualized using confocal laser scanning microscopy (CLSM) (Figure 4a). Cell nuclei were counterstained with DAPI, and cell morphology was shown in differential interference contrast (DIC) images. The nanoparticles were rapidly internalized within 30 min and continued to localize in the cytoplasm for up to 8 h of incubation. No difference in cellular uptake was observed in the additional incubation after 8 h (data not shown). The *in vitro* anticancer activity of the 17-AAG-loaded rHG-TOS (17-AAG/rHG-TOS) nanoparticles was examined in SCC cells. Cytotoxicities of free 17-AAG, rHG-TOS nanoparticles, and 17-AAG/rHG-TOS nanoparticles were determined in a 17-AAG dose-dependent manner. At an equivalent dose of 17-AAG, 17-AAG/rHG-TOS nanoparticles exhibited an ~10% higher cytotoxicity in SCC

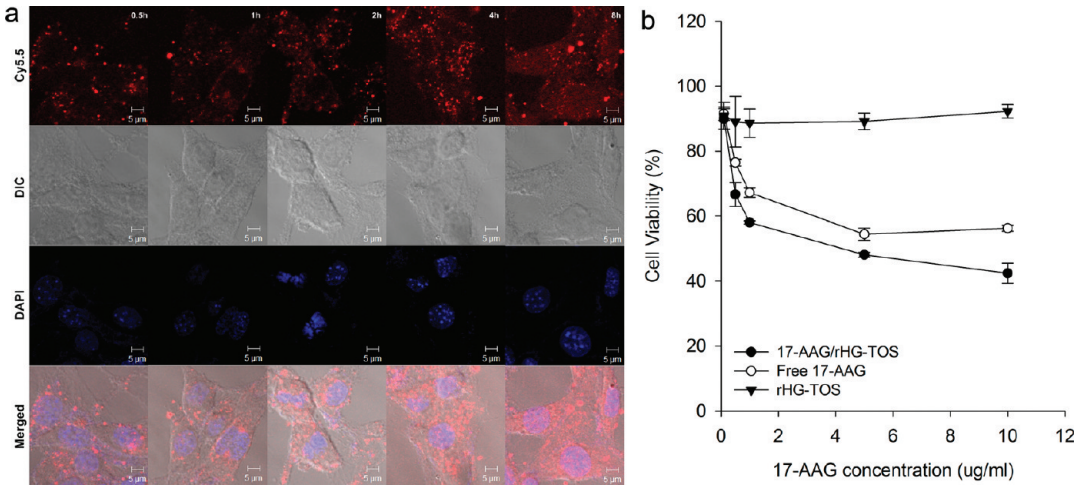

Figure 4. (a) Cellular uptake and distribution of rHG-TOS nanoparticles monitored using CLSM. The rHG-TOS nanoparticles were labeled with Cy5.5 dye (red, top), cell morphologies were visualized in DIC images (gray, second from top), nuclei were counterstained with DAPI (blue, third from top), and the images were merged (bottom). (b) Anticancer effects of 17-AAG-loaded rHG-TOS nanoparticles in SCC cells (data expressed as mean ± SD of three independent experiments with four replicates). (▼) rHG-TOS; (○) free 17-AAG; (●) 17-AAG-loaded rHG-TOS.

cells than did free 17-AAG, while the unloaded rHG-TOS showed an ~10% reduction in cell viability without dose dependency (Figure 4b). The anticancer effects were evaluated to normalize in the MCF-7 and MDA-MB-231 cell lines (Figures S3a, b). The 10% difference between free 17-AAG and 17-AAG/rHG-TOS nanoparticles was not large; however, the effects of nanoparticles on the drug activity should be considered in addition to the release profile. Since ~50% of 17-AAG was released from the rHG-TOS nanoparticles during the first 24 h, as shown in the *in vitro* release profile (Figure 3a), the cytotoxicities of 17-AAG/rHG-TOS nanoparticles might be attributed to the released amounts of 17-AAG from the nanoparticles, even though the release behavior of 17-AAG in cells differs from that in the test tubes.

The advantage of nanoparticles for anticancer drug delivery mainly lies in passive targeting to the tumor tissue *via* the EPR effect.[31] The distribution, passive targeting to the tumor through the EPR effect, and the residence time in the mouse model were observed and visualized using a noninvasive live animal imaging technique after a systemic injection of Cy5.5-labeled rHG-TOS nanoparticles though the tail vein. After the injection, the NIR fluorescence intensity of the rHG-TOS was detected at predetermined points in time. Nanoparticle accumulation in the tumor was observed within 1 h and continued to increase up to 6 h, after which a slight decrease in the intensity was observed at 12 h postinjection and maintained for 1 day (Figure 5a). The intensity kept decreasing during the observation. A quantitative analysis of the nanoparticle distribution was performed by measuring the fluorescence intensities in the region of interest (ROI) (Figure 5b). ROI intensity at 1 h postinjection was considered as 100%, and other points were expressed as relative intensities. In order to avoid autofluorescence from the tumor, fluorescence intensity in the tumor was measured before the injection. Since photobleaching of Cy5.5 is one factor that causes continuously decreased fluorescence intensity with time, the tumor to background ratios (TBR) were calculated as shown in Figure 5c.[32] TBR increased for one day, maintained a stable value from one day to two days, and then continuously declined. These results reveal rapid uptake and long-term retention of rHG-TOS nanoparticles in the tumor region during the continuous elimination of the nanoparticles in the body. Tumor targetability and elimination of rHG-TOS nanoparticles can be confirmed through the biodistribution study; however, it is difficult to monitor organ distributions using the live animal imaging.[1,33] Therefore, *ex vivo* observations were performed 24 h after a single injection. Figure 5d exhibits the strongest fluorescence intensity at the tumor compared to those of the liver, lung, kidney, spleen, heart, and muscle. A quantitative analysis revealed at least 2-fold greater fluorescence intensity at the tumor in comparison to other organs, supporting the tumor targeting ability of rHG-TOS nanoparticles (Figure 5e). On the basis of these results, it is concluded that the rHG-TOS nanoparticles are found to passively target the tumor tissue *via* the EPR effect and remain at the tumor region for sufficient time to complete the drug release.

Despite the importance of biodistribution, penetration through tissue, phagocytosis, and endocytosis of nanomaterials, little is known about metabolism of nanomaterials because of the difficulty in detection and quantification of the metabolites of nanomaterials. Chromatography, mass spectrometry, and NMR, the most commonly used analytical methods, are not critical to determine the metabolism of nanomaterials,

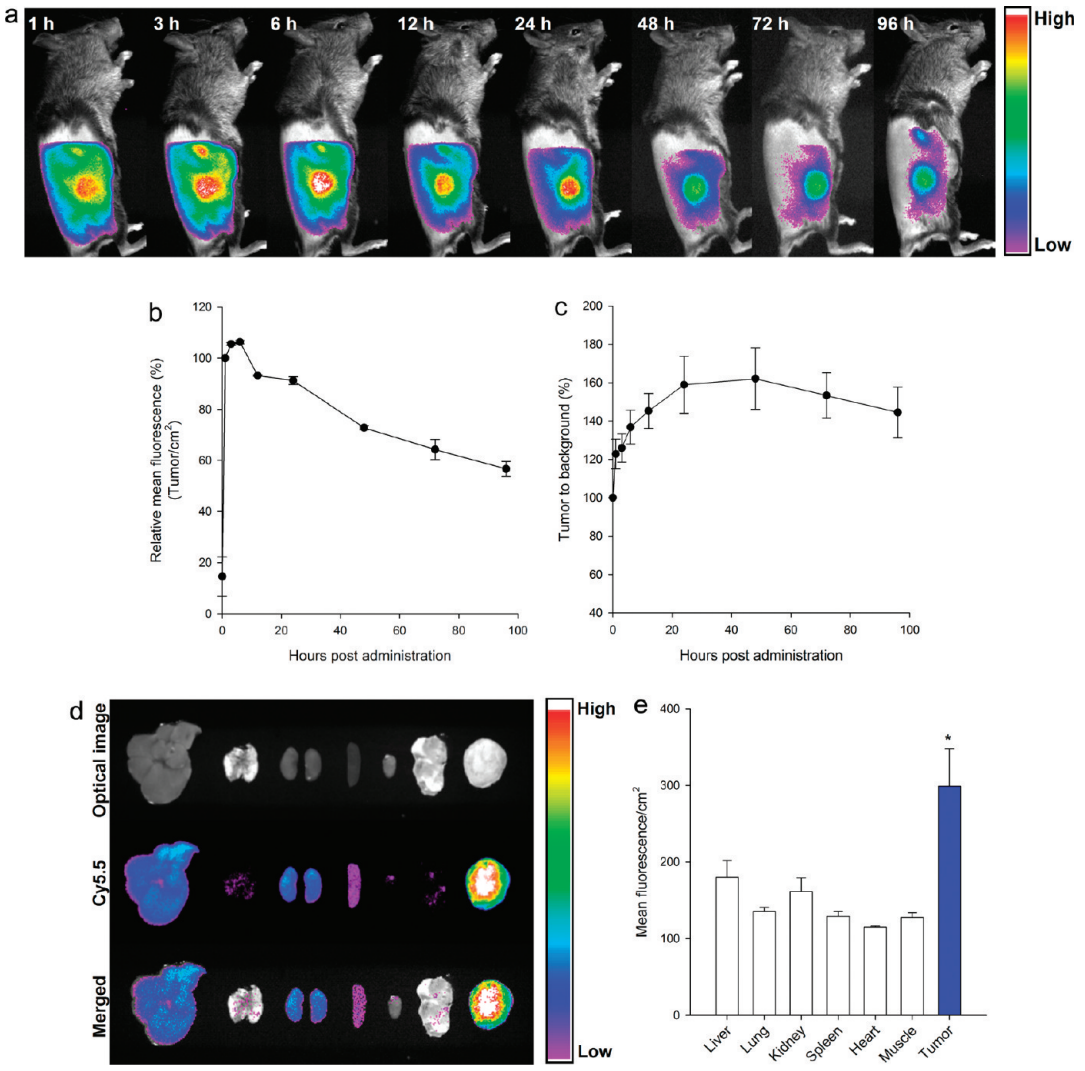

Figure 5. (a) Distribution of Cy5.5-labeled rHG-TOS nanoparticles in the tumor-bearing mice after a single systemic injection. (b) Relative mean fluorescence in the tumor tissue determined according to the mean fluorescence in the ROI (data expressed as mean ± SE, $n = 5$). (c) Residence time and elimination of rHG-TOS of the tumor (data expressed as mean ± SD). (d) *Ex vivo* examination to visualize the tumor targeting ability of rHG-TOS nanoparticles. Major organs, muscle, and tumor tissue were isolated one day after administration (liver, lung, kidney, spleen, heart, muscle, and tumor; left to right). (e) Quantitative analysis of rHG-TOS nanoparticles in the major organs (*$p < 0.001$, ANOVA, tumor *vs* other organs and muscle; data expressed as mean ± SD).

even though they are general methodologies for micromaterials. Therefore, nanoparticles require an additional technique to detect and quantify the metabolized products. Continuous studies have proposed that the surface characteristics of nanoparticles are closely related with exposure and uptake, translocation and metabolism, and elimination of nanoparticles in biological systems.[34] The toxicity of nanoparticles is detoxified through an activation of the liver, and most nanoparticles are eliminated *via* a glomerular filtration if their overall molecular weight is lower than the renal cutoff. As shown in Figure 5d, the intensity of rHG-TOS was slightly high in the liver and kidney in comparison with other major organs except the tumor, demonstrating that the rHG-TOS nanoparticles might be eliminated through the kidney and detoxified in the liver. The liver and kidney toxicity after the systemic administration of rHG-TOS nanoparticles should be further evaluated, although the total amount of nanoparticles seems not to be overdosed.

The effects of the nanoparticles on the efficacy of 17-AAG were investigated in terms of the administration dose and frequency. For preparation of the injection solution, free 17-AAG was first dissolved in DMSO and diluted with PBS, and the unloaded nanoparticles and 17-AAG/rHG-TOS nanoparticles were suspended in PBS. The administration doses for free 17-AAG and 17-AAG/rHG-TOS nanoparticles were 10 and 5 mg/kg per mouse, respectively. PBS was injected as vehicle, and unloaded rHG-TOS nanoparticles were used as a negative control. All of the samples were systemically injected into the tumor-bearing mice three times per

week. After the sixth injection, the tumor volume in the group of free 17-AAG was increased 20 times relative to the initial volume, whereas that of 17-AAG/rHG-TOS nanoparticles was increased 15 times (Figure 6). In order to evaluate whether the use of nanoparticles reduced the administration frequency, we injected 17-AAG/rHG-TOS nanoparticles every four days at a 17-AAG dose of 10 mg/kg. At the end of administration, the tumor volume increased 7 times, which is one-third compared to the free 17-AAG after the injections at the same dose of 17-AAG. As shown in Figure 6, 17-AAG/rHG-TOS nanoparticles exhibited strong anticancer effects even with a low dose of 17-AAG and a long-term interval in comparison with the effects of free 17-AAG. This is in part due to the passive targeting ability of nanoparticles through the EPR effects, through which 17-AAG may be accumulated at the tumor region at high local concentration even with low doses and low frequency.

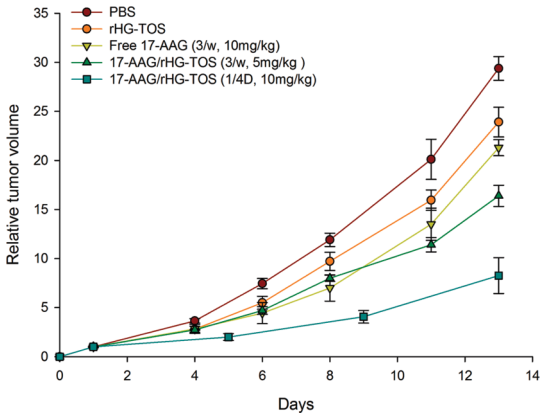

Figure 6. Anticancer effects of 17-AAG-loaded rHG-TOS nanoparticles in SCC tumor-bearing mice ($p < 0.001$, ANOVA, free 17-AAG *vs* 17-AAG-loaded rHG-TOS; data expressed as mean ± SE, $n = 5$). Symbols on the plots represent one day postadministration (red ●) PBS (vehicle); (orange ●) rHG-TOS; (▼) free 17-AAG, three times per week at 10 mg/kg; (blue ■) 17-AAG-loaded rHG-TOS, three times per week at 5 mg/kg; (purple ■) 17-AAG-loaded rHG-TOS, every four days at 10 mg/kg.

Since it has been reported that natural killer cells (NK cells), a component of the innate immune system, play a crucial role in tumor rejection, changes in NK cell population in tumor, blood, and draining lymph node (DLN) were monitored.[35] The percentage of NK cells did not change significantly after administration of 17-AAG/rHG-TOS nanoparticles (Figure 7a), demonstrating that the retarded tumor growth was due to the anticancer activity of 17-AAG, but not through NK cell activation. To determine the immunogenicity of rHG-TOS nanoparticles, the percentage of lymphocytes in the blood, tumor, and DLN was measured using flow cytometry. Investigation of

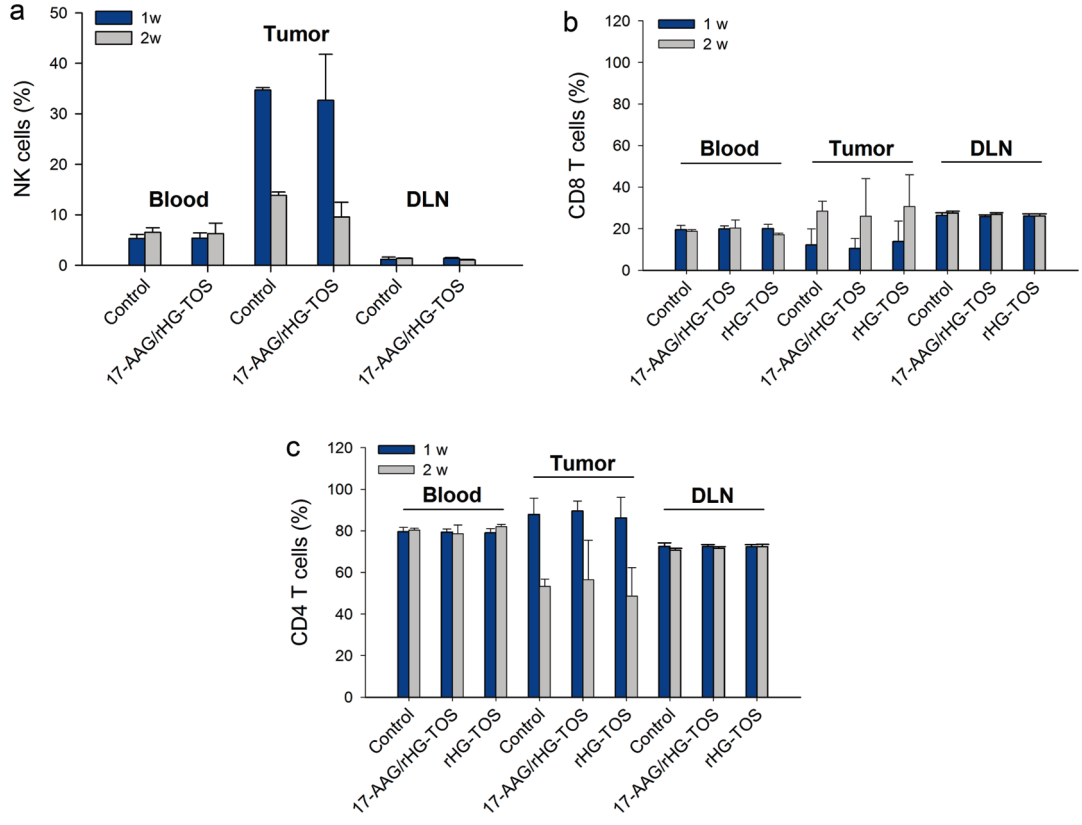

Figure 7. Immunogenecity of 17-AAG-loaded rHG-TOS nanoparticles in SCC tumor-bearing mice. (a) Percentage of CD3-DX5+ NK cells in blood, tumor, and DLN at one and two weeks after the administration of 17-AAG/rHG-TOS nanoparticles was measured by flow cytometry. (b) $CD8^+$ and (c) $CD4^+$ T cell populations in blood, tumor, and DLN at one and two weeks after administration of 17-AAG/rHG-TOS nanoparticles were measured by flow cytometry. The nanoparticles and vehicle were injected every 4 days at a 17-AAG dose of 10 mg/kg.

$CD8^+$ and $CD4^+$ (Figure 7b,c) populations revealed that rHG-TOS was nonimmunogenic when injected systemically. Taken together, these data demonstrate that rHG-TOS is a safe and nonimmunogenic biomaterial when utilized as a drug delivery system for 17-AAG, primarily *via* the increase in targeted delivery of 17-AAG at the tumor sites and allowing sustained drug release.

CONCLUSION

New self-assembled nanoparticles based on rHG for 17-AAG delivery were successfully developed through the introduction of hydrophobic α-TOS. The rHG-TOS nanoparticles exhibit advantages of enhancing the therapeutic efficacy of 17-AAG through the passive targeting of the tumor with long residence time and reduction in the administration dose and frequency. In addition, rHG-TOS is a biocompatible and bioeliminable material in terms of its degradability and nonimmunogenicity. Consequently, rHG-TOS has the potential to deliver hydrophobic anticancer agents with high loading efficiency and stability. To our knowledge, this is the first study to use rHG for hydrophobic drug delivery and Hsp90 inhibitor, 17-AAG, as an anticancer agent. Despite future challenges regarding the mechanisms of the anticancer effects, optimization of administration dosage, evaluation of liver and kidney toxicity, and the nanoparticles' stability in blood, the present data provide promising applications of rHG-TOS as an efficient and safe anticancer drug carrier. Current work will promote further applications of rHG-TOS for versatile anticancer drug delivery and of biologically active anticancer agents in other drug delivery systems.

METHODS

Materials. RHG (100 kDa) was purchased from Fibrogen, Inc. (San Francisco, CA). EDC (1-ethyl-3-[3-dimethylaminopropyl]carbodiimide hydrochloride), NHS (*N*-hydroxysuccinimide), α-TOS (D-α-tocopheryl succinate), DPH (1,6-diphenyl-1,3,5-hexatriene), KBr (potassium bromide, FT-IR grade), and DMSO (NMR grade) were obtained from Sigma-Aldrich Co. (St. Louis, MO). 17-(Allylamino)-17-demethoxygeldanamycin (17-AAG) was from LC Laboratories (Woburn, MA); acetonitrile and methanol (HPLC grade) were from Fisher Scientific Korea (Seoul, Republic of Korea); SCC (squamous cell carcinoma), MDA-MB-231, and MCF-7 were from the American Type Culture Collection (Rockville, MD); cyanine 5.5 NHS ester (Cy5.5) was from Amersham Biosciences (Piscataway, NJ); the dialysis membrane was purchased from Spectrum Laboratories, Inc. (Rancho Dominguez, CA); the C3H mice were from Orient Bio Inc. (Seongnam-Si, Gyeonggi-Do, Republic of Korea). Allophycocyanin (APC)-conjugated anti-CD8 (53-6.7) and PE-conjugated anti-CD4 (GK1.5) mAb were purchased from eBioscience (San Diego, CA). The ultrapure deionized water (DW) was produced using a Millipore purification system. All other reagents were of analytical grade.

Preparation of rHG-TOS. The conjugate of rHG-TOS was prepared through formation of amide bonds between the primary amine of rHG and the carboxyl group of α-TOS *via* the EDC/NHS reaction as previously reported.[1] In order to activate the carboxylates, EDC was dissolved in an activation buffer (0.1 M MES, 0.5 M NaCl, pH 6.0) at a final concentration of 500 mM, and α-TOS was prepared in methanol at a final concentration of 100 mM. The stocks of EDC and α-TOS were diluted with 5-fold volume of the activation buffer and 3-fold volume of methanol, respectively, and then they were mixed at a volume ratio of 6:4 for preparing a mixture containing 50 mM EDC and 10 mM α-TOS. After 30 min of reaction, NHS was added at a final concentration of 5 mM, and the mixture was reacted for 4 h with slow stirring. To inactivate EDC, 2-mercaptoethanol was added at a final concentration of 20 mM, and the solution was mixed with 2 × PBS (0.2 M, 0.3 M NaCl, pH 7.4) containing 50 μM rHG at a ratio of 1 to 1. The resulting solution was stirred for 16 h at room temperature. After the reaction, the conjugate was purified through 24 h of dialysis (MWCO 1 kDa) against 40% methanol and an additional 48 h with continuously decreasing methanol until the buffer reached 100% water. The purified rHG-TOS was freeze-dried and stored under vacuum at −20 °C until use.

Characterization. *Critical Aggregation Concentration.* DPH was dissolved in methanol to prepare a 0.4 mM stock solution, and rHG-TOS was dissolved in water with serial dilution from 125 to 0.49 μg/mL. The stock solution of DPH was mixed with the samples of rHG-TOS at a final DPH concentration of 0.004 mM prior to sonication at 30% amplification for 20 s. As a negative control, samples were prepared through the same procedure in the absence of DPH. After 24 h at room temperature, fluorescence intensities of the samples were measured with excitation at 355 nm and emission at 428 nm using a UV/vis fluorescence spectrophotometer (SpectraMax M2^e, Molecular Devices; Sunnyvale, CA). The differences between the samples with and without DPH were considered based on the mean fluorescence intensities.

TEM. Samples were prepared from an aqueous solution of rHG-TOS at concentrations greater than the CAC and were dispersed by sonication. One drop of the solution was dried on a carbon grid and stained with osmium tetroxide. The morphological characteristics of rHG-TOS were visualized using a TEM (Philips CM-30, Philips Electron Optics; Eindhoven, Netherlands).

Size. The mean diameters and size distributions were determined with dynamic light scattering using a Zetasizer (NanoZS, Malvern Instruments; Worcestershire, UK). The rHG-TOS nanoparticles were dissolved and dispersed in DW at a concentration of 0.5 mg/mL.

Preparation of 17-AAG-Loaded Nanoparticles. DMSO was chosen as a cosolvent to dissolve rHG-TOS and 17-AAG, which were then separately dissolved in DMSO. The rHG-TOS solution was first sonicated at 30% amplification for 20 s and mixed with 17-AAG. The mixture was sonicated again with the same conditions, and the resulting mixture was dialyzed (MWCO 1 kDa) against water for 5 h with frequent exchange of pure water. After that, the 17-AAG-loaded rHG-TOS nanoparticles were lyophilized and maintained under vacuum at −20 °C until use. The loaded amount of 17-AAG in the nanoparticles was determined using HPLC (1525 dual pump, Waters; Milford, MA) equipped with a UV detector and a C_{18} column. The column was equilibrated with a mobile phase (31% ACN, 43% methanol, 26% water), and the samples were eluted in an isocratic condition of the mobile phase at a flow rate of 1 mL/min and detected at 254 nm. LC% and LE% were calculated as LC% = mass of 17-AAG in nanoparticles/mass of 17-AAG-loaded nanoparticles × 100 and LE% = mass of 17-AAG loaded in nanoparticles/mass of 17-AAG added × 100, respectively.[3]

17-AAG Release Study. The dialysis method was used for the *in vitro* 17-AAG release experiments. The 17-AAG-loaded rHG-TOS nanoparticles were dissolved in PBS at a final concentration of 3 mg/mL, and the solution was sealed in a dialysis bag (MWCO 1 kDa), which was immersed into 10 mL of PBS (0.1 M, 0.15 M NaCl, pH 7.4) in a conical tube. The tube was placed in a shaking water bath at 37 °C and shaken horizontally at 100 rpm.

The release buffer in the tube was replaced with fresh PBS at the predetermined points in time. The released 17-AAG contents were quantified using HPLC as described above.

***In Vitro* Studies.** *Cell Culture.* SCC cells were maintained in RPMI 1640, 10% FBS, and penicillin (100 IU/ml)/streptomycin (100 μg/mL) at 37 °C with 5% CO_2 and cultured to 80% confluence.

Cellular Uptake. Cy5.5 was conjugated to the residual amine groups of rHG-TOS through an amide bond according to the manufacturer's protocol. SCC cells were seeded onto 60 mm dishes at a density of 1×10^6 cells/dish and then incubated for 24 h. After the incubation, Cy5.5-labeled rHG-TOS was treated to the cells at a final concentration of 50 μg/mL, and the cells were washed three times with PBS at the predetermined points in time. Then, the cellular uptake was observed using a confocal microscope (LSM510 META NLO, Carl Zeiss Jena GmbH, Germany; Korea Basic Science Institute, Chuncheon Center, Chuncheon, Korea).

In Vitro Studies. SCC cells were seeded onto 24-well plates at a density of 1×10^4 cells/well. After 24 h of incubation, the culture media was replaced with 500 μL of fresh media containing 17-AAG-loaded rHG-TOS nanoparticles, free 17-AAG, or unloaded nanoparticles. The 17-AAG-loaded nanoparticles were serially diluted in the media to produce a final 17-AAG concentration range from 10 to 0.1 μg/mL. As controls, equivalent doses of free 17-AAG and unloaded nanoparticles were administered to the cells. After 24 h of incubation, the cells were washed with PBS and the cell viability was determined using an MTT assay. The cell viabilities were measured three times with four replicates.

Biodistribution. *Tumor Model.* All animal experiments were conducted under an animal protocol approved by the Institutional Animal Care and Use Committee at the Hanyang University, Korea. SCC cells grown to 80% confluence were trypsinized and suspended in PBS at a concentration of 4.0×10^7 cells/mL. Fifty microliters of cells was inoculated into the left hind flank of six-week-old C3H mice after anaesthetizing with ketamine and xylazine (100 mg/kg). Tumor volume was calculated as $V = 0.5ab^2$, where a and b are the longest and shortest diameters, respectively, of tumors measured using vernier calipers.[36]

Cy5.5-rHG-TOS Injection. The tumor model was prepared as described above, and the mice were randomly separated into control and test groups when the tumor volumes reached ~200 mm^3. Cy5.5-labeled rHG-TOS was injected through the tail vein at an administration dose of 1 mg suspended in 100 μL of PBS.

Body Distribution. The distribution of nanoparticles was visualized and quantitatively analyzed using a Kodak Image Station at the predetermined time points (Kodak Image Station 4000MM, Eastman Kodak Company, Scientific Imaging Systems; New Haven, CT). The mean fluorescence intensity (MFI) at the tumor was determined in the ROI and was expressed as MFI/cm^2. The tumor to background intensity (TBI) was calculated as TBI = MFI in the ROI of tumor/MFI in the ROI of skin × 100.

Ex Vivo Examination. The tumor tissue and internal organs, including liver, lung, kidney, spleen, heart, and muscle, were isolated 24 h post intravenous injection of Cy5.5-labeled rHG-TOS nanoparticles. The MFIs of the tumor and organs were measured and calculated using the equation described above.

***In Vivo* Anticancer Effects.** When the tumor volumes reached ~70 mm^3, the mice were randomly divided into six groups of PBS, unloaded rHG-TOS nanoparticles, free 17-AAG (1), and 17-AAG/rHG-TOS nanoparticles (2 and 3): (1) three times per week at a 17-AAG dose of 10 mg/kg; (2) three times per week at a dose of 5 mg/kg; and (3) every four days at a dose of 10 mg/kg. All treatments were injected into the mice through the tail vein. The tumor volumes were measured and calculated with the equation provided above.

Immune Profiling. Draining lymph nodes were minced with frosted glass slides, and tumor mass was taken out and passed through a 70 μm pore-size nylon cell strainer (BD Falcon 352350; BD Biosciences, Bedford, MA) using a 15 mL syringe plunger to disperse clumps to remove debris. Isolated single cells were resuspended in 100 μL of FACS buffer (PBS containing 2% FBS and 0.02% sodium azide) and incubated with anti-CD16/CD32 mAb to block FcγRIII/II. Without washing, cells were incubated with mAb for 20 min at 4 °C. After washing with FACS buffer, cells were fixed with 200 μL of 1% paraformaldehyde in PBS. Flow cytometry was performed using FACSCalibur (BD Biosciences, San Diego, CA), and the data were analyzed with CellQuest software (BD PharMingen, San Jose, CA). Fifty thousand lymphocyte populations gated by forward-/side-scatter were analyzed.

Acknowledgment. This work was partially supported by grants from the Korea Science and Engineering Foundation (2010K001247, 2010K001350) and World Class University Program (WCU, R332010000100360) through the National Research Foundation of Korea funded by the Ministry of Education, Science, and Technology. K.-M.L. and her group were supported by a grant from KICOS through the Korean Ministry of Science & Technology (K20704000007-10A0500-00710 and K20902001448-10E0100-03010) and the Innovative Research Institute for Cell Therapy (A062260).

Supporting Information Available: FT-IR and ^{1}H NMR spectra of rHG-TOS, table for the optimization of rHG-TOS conjugation, cryo-TEM micrograph of rHG-TOS nanoparticle, and anticancer effects in MCF-7 and MDA-MB-231 cells are available. This material is available free of charge *via* the Internet at http://pubs.acs.org.

REFERENCES AND NOTES

1. Hwang, H.-Y.; Kim, I.-S.; Kwon, I. C.; Kim, Y.-H. Tumor Targetability and Antitumor Effect of Docetaxel-Loaded Hydrophobically Modified Glycol Chitosan Nanoparticles. *J. Controlled Release* **2008**, *128*, 23–31.
2. Li, L.; Tang, F.; Liu, H.; Liu, T.; Hao, N.; Chen, D.; Teng, X.; He, J. In Vivo Delivery of Silica Nanorattle Encapsulated Docetaxel for Liver Cancer Therapy with Low Toxicity and High Efficacy. *ACS Nano* **2010**, *4*, 6874–6882.
3. Du, Y.-Z.; Weng, Q.; Yuan, H.; Hu, F.-Q. Synthesis and Antitumor Activity of Stearate-G-Dextran Micelles for Intracellular Doxorubicin Delivery. *ACS Nano* **2010**, *4*, 6894–6902.
4. Won, Y.-W.; Kim, Y.-H. Recombinant Human Gelatin Nanoparticles as a Protein Drug Carrier. *J. Controlled Release* **2008**, *127*, 154–161.
5. Neuzil, J. Vitamin E Succinate and Cancer Treatment: A Vitamin E Prototype for Selective Antitumour Activity. *Br. J. Cancer* **2003**, *89*, 1822–1826.
6. Birringer, M.; EyTina, J. H.; Salvatore, B. A.; Neuzil, J. Vitamin E Analogues as Inducers of Apoptosis: Structure-Function Relation. *Br. J. Cancer* **2003**, *88*, 1948–1955.
7. Wang, X.-F.; Dong, L.; Zhao, Y.; Tomasetti, M.; Wu, K.; Neuzil, J. Vitamin E Analogues as Anticancer Agents: Lessons from Studies with A-Tocopheryl Succinate. *Mol. Nutr. Food Res.* **2006**, *50*, 675–685.
8. Kamal, A.; Boehm, M. F.; Burrows, F. J. Therapeutic and Diagnostic Implications of Hsp90 Activation. *Trends Mol. Med.* **2004**, *10*, 283–290.
9. Powers, M. V.; Workman, P. Inhibitors of the Heat Shock Response: Biology and Pharmacology. *FEBS Lett.* **2007**, *581*, 3758–3769.
10. Whitesell, L.; Lindquist, S. L. Hsp90 and the Chaperoning of Cancer. *Nat. Rev. Cancer* **2005**, *5*, 761–772.
11. Solit, D. B.; Chiosis, G. Development and Application of Hsp90 Inhibitors. *Drug Discovery Today* **2008**, *13*, 38–43.
12. Chiosis, G.; Neckers, L. Tumor Selectivity of Hsp90 Inhibitors: The Explanation Remains Elusive. *ACS Chem. Biol.* **2006**, *1*, 279–284.
13. Kamal, A.; Thao, L.; Sensintaffar, J.; Zhang, L.; Boehm, M. F.; Fritz, L. C.; Burrows, F. J. A High-Affinity Conformation of Hsp90 Confers Tumour Selectivity on Hsp90 Inhibitors. *Nature* **2003**, *425*, 407–410.
14. Li, Y.; Zhang, T.; Schwartz, S. J.; Sun, D. New Developments in Hsp90 Inhibitors as Anti-Cancer Therapeutics: Mechanisms,

Clinical Perspective and More Potential. *Drug Resist. Update* **2009**, *12*, 17–27.
15. Workman, P.; Burrows, F.; Neckers, L. E. N.; Rosen, N. Drugging the Cancer Chaperone Hsp90. *Ann. N.Y. Acad. Sci.* **2007**, *1113*, 202–216.
16. Roe, S. M.; Prodromou, C.; O'Brien, R.; Ladbury, J. E.; Piper, P. W.; Pearl, L. H. Structural Basis for Inhibition of the Hsp90 Molecular Chaperone by the Antitumor Antibiotics Radicicol and Geldanamycin. *J. Med. Chem.* **1999**, *42*, 260–266.
17. Mimnaugh, E. G.; Chavany, C.; Neckers, L. Polyubiquitination and Proteasomal Degradation of the P185(C-Erbb-2) Receptor Protein-Tyrosine Kinase Induced by Geldanamycin. *J. Biol. Chem.* **1996**, *271*, 22796–22801.
18. Neckers, L.; Schulte, T. W.; Mimnaugh, E. Geldanamycin as a Potential Anti-Cancer Agent: Its Molecular Target and Biochemical Activity. *Invest. New Drugs* **1999**, *17*, 361–373.
19. Heath, E.; Gaskins, M.; Pitot, H.; Pili, R.; Tan, W.; Marschke, R.; Liu, G.; Hillman, D.; Sarkar, F.; Sheng, S.; *et al.* A Phase II Trial of 17-Allylamino-17-Demethoxygeldanamycin in Patients with Hormone-Refractory Metastatic Prostate Cancer. *Clin. Genitourin. Cancer* **2005**, *4*, 138–141.
20. Ronnen, E.; Kondagunta, G.; Ishill, N.; Sweeney, S.; DeLuca, J.; Schwartz, L.; Bacik, J.; Motzer, R. A Phase II Trial of 17-(Allylamino)-17-Demethoxygeldanamycin in Patients with Papillary and Clear Cell Renal Cell Carcinoma. *Invest. New Drugs* **2006**, *24*, 543–546.
21. Zhang, H.; Neau, S. H. In Vitro Degradation of Chitosan by Bacterial Enzymes from Rat Cecal and Colonic Contents. *Biomaterials* **2002**, *23*, 2761–2766.
22. Wu, W.; Li, R.; Bian, X.; Zhu, Z.; Ding, D.; Li, X.; Jia, Z.; Jiang, X.; Hu, Y. Covalently Combining Carbon Nanotubes with Anticancer Agent: Preparation and Antitumor Activity. *ACS Nano* **2009**, *3*, 2740–2750.
23. Fox, M. E.; Szoka, F. C.; Fréchet, J. M. J. Soluble Polymer Carriers for the Treatment of Cancer: The Importance of Molecular Architecture. *Acc. Chem. Res.* **2009**, *42*, 1141–1151.
24. Olsen, D.; Yang, C.; Bodo, M.; Chang, R.; Leigh, S.; Baez, J.; Carmichael, D.; Perälä, M.; Hämäläinen, E.-R.; Jarvinen, M.; *et al*. Recombinant Collagen and Gelatin for Drug Delivery. *Adv. Drug Delivery Rev.* **2003**, *55*, 1547–1567.
25. Cavalieri, F.; Postma, A.; Lee, L.; Caruso, F. Assembly and Functionalization of DNA−Polymer Microcapsules. *ACS Nano* **2009**, *3*, 234–240.
26. Zhou, H.; Yu, W.; Guo, X.; Liu, X.; Li, N.; Zhang, Y.; Ma, X. Synthesis and Characterization of Amphiphilic Glycidol−Chitosan−Deoxycholic Acid Nanoparticles as a Drug Carrier for Doxorubicin. *Biomacromolecules* **2010**, *11*, 3480–3486.
27. Dong, L. F.; Low, P.; Dyason, J. C.; Wang, X. F.; Prochazka, L.; Witting, P. K.; Freeman, R.; Swettenham, E.; Valis, K.; Liu, J.*et al*. [Alpha]-Tocopheryl Succinate Induces Apoptosis by Targeting Ubiquinone-Binding Sites in Mitochondrial Respiratory Complex II. *Oncogene* **2008**, *27*, 4324–4335.
28. Barzegar-Jalali, M.; Adibkia, K.; Valizadeh, H.; Shadbad, M.; Nokhodchi, A.; Omidi, Y.; Mohammadi, G.; Nezhadi, S.; Hasan, M. Kinetic Analysis of Drug Release from Nanoparticles. *J. Pharm. Pharm. Sci.* **2008**, *11*, 167–177.
29. Guo, W.; Reigan, P.; Siegel, D.; Zirrolli, J.; Gustafson, D.; Ross, D. Formation of 17-Allylamino-Demethoxygeldanamycin (17-Aag) Hydroquinone by Nad(P)H:Quinone Oxidoreductase 1: Role of 17-AAG Hydroquinone in Heat Shock Protein 90 Inhibition. *Cancer Res.* **2005**, *65*, 10006–10015.
30. Guo, W.; Siegel, D.; Ross, D. Stability of the Hsp90 Inhibitor 17AAG Hydroquinone and Prevention of Metal-Catalyzed Oxidation. *J. Pharm. Sci.* **2008**, *97*, 5147–5157.
31. Lee, S.-M.; Ahn, R. W.; Chen, F.; Fought, A. J.; O'Halloran, T. V.; Cryns, V. L.; Nguyen, S. T. Biological Evaluation of Ph-Responsive Polymer-Caged Nanobins for Breast Cancer Therapy. *ACS Nano* **2010**, *4*, 4971–4978.
32. Dempsey, G. T.; Bates, M.; Kowtoniuk, W. E.; Liu, D. R.; Tsien, R. Y.; Zhuang, X. Photoswitching Mechanism of Cyanine Dyes. *J. Am. Chem. Soc.* **2009**, *131*, 18192–18193.
33. Rosenthal, E. L.; Kulbersh, B. D.; King, T.; Chaudhuri, T. R.; Zinn, K. R. Use of Fluorescent Labeled Anti−Epidermal Growth Factor Receptor Antibody to Image Head and Neck Squamous Cell Carcinoma Xenografts. *Mol. Cancer Ther.* **2007**, *6*, 1230–1238.
34. Liang, X. J.; Chen, C.; Zhao, Y.; Jia, L.; Wang, P. C. Biopharmaceutics and Therapeutic Potential of Engineered Nanomaterials. *Curr. Drug Metab.* **2008**, *9*, 697–709.
35. Raulet, D. H.; Guerra, N. Oncogenic Stress Sensed by the Immune System: Role of Natural Killer Cell Receptors. *Nat. Rev. Immunol.* **2009**, *9*, 568–580.
36. Won, Y.-W.; Yoon, S.-M.; Lee, K.-M.; Kim, Y.-H. Poly(Oligo-D-Arginine) with Internal Disulfide Linkages as a Cytoplasm-Sensitive Carrier for siRNA Delivery. *Mol. Ther.* **2010**, *19*, 372–380.